Atopic Dermatitis Detection with a Compact Ku-Band CSRR-Based Sensor

Atopic Dermatitis Detection with a Compact Ku-band CSRR-Based Sensor

Alessandra Di Florio Di Renzo
DEI "Guglielmo Marconi"
University of Bologna
Bologna, Italy
alessandra.diflorio3@unibo.it

Simone Trovarello
DEI "Guglielmo Marconi"
University of Bologna
Bologna, Italy
simone.trovarello2@unibo.it

Diego Masotti
DEI "Guglielmo Marconi"
University of Bologna
Bologna, Italy
diego.masotti@unibo.it

Marco Tartagni
DEI "Guglielmo Marconi"
University of Bologna
Cesena, Italy
marco.tartagni@unibo.it

Alessandra Costanzo
DEI "Guglielmo Marconi"
University of Bologna
Bologna, Italy
alessandra.costanzo@unibo.it

***Abstract*—This work presents a microwave-based system for monitoring superficial skin fissures, characteristic of Atopic Dermatitis (AD). The proposed solution utilizes a miniaturized Complementary Split Ring Resonator (CSRR) operating at 16 GHz, excited by a coupled open-ended microstrip line. The sensor is compact, non-invasive, and electrode-less. The high operating frequency is selected to ensure that the resonator near-field interaction is confined to the superficial, non-vascularized skin layers, namely the *stratum corneum*. As a result, the resonator fringing field predominantly interacts with AD-induced skin fissures. Depending on the dimensions and severity of the damage, variations in the skin effective complex permittivity of the affected layers can be detected by monitoring changes in the system's reflection coefficient S_{11} and E-field penetration. The novel sensor concept is designed and initially validated through electromagnetic (EM) simulations, demonstrating high sensitivity to 3-D variations in fissure characteristics. The selective interaction with superficial layers is confirmed only by analyzing the electromagnetic field distribution across them, which is corroborated by the corresponding variations in the amplitude and phase of S_{11} at the sensing interface. This approach provides a low-cost and effective solution for detecting AD-related skin damage and distinguishing between different severity levels of the condition.**

***Index Terms*—Atopic Dermatitis, CSRR, microwave sensing.**

I. Introduction

Atopic Dermatitis (AD) is a common skin disease that affects approximately 230 million people worldwide. One of the primary characteristics of AD is the significant impairment of the *stratum corneum* (SC), the outermost layer of the epidermis. SC plays a crucial role in protecting the skin and preventing transepidermal water loss (TEWL). In AD, SC becomes structurally and functionally compromised, leading to increased TEWL and skin dehydration, as illustrated in Fig. 1. Clinically, this results in pruritus, dry skin, inflammation, and an increased risk of infections [1]. Planar microwave sensors are promising candidates for detecting AD because of their non-invasive nature, the use of non-ionizing radiation, and cost-effectiveness. Most existing skin sensors reported in the literature can classify skin hydration levels only into broad categories such as hydrated or dehydrated [2], [3], [4]. However, these classifications are not accurate or specific enough to detect biomarkers associated with AD, since the skin is considered a single homogeneous layer, without considering the multilayered structure, including SC, epidermis (EP), and dermis (DR). Some studies specifically focus on the SC, recognizing its key role in skin barrier function and water retention [5], [6], [7], [8]. However, the literature lacks clear hydration thresholds for AD-affected skin, making it hard to distinguish normal from pathological dryness. In [9], an interdigitated capacitive sensor for detecting AD biomarkers is presented. Nevertheless, the low operating frequency and the lack of structural alterations typical of AD in the SC model may affect accuracy. Given the dimensions of the thin layer of SC, frequencies in the high microwave range can improve the resolution in the AD detection. Moreover, a detailed description of the skin slab in the presence of AD may enhance the detection mechanism.

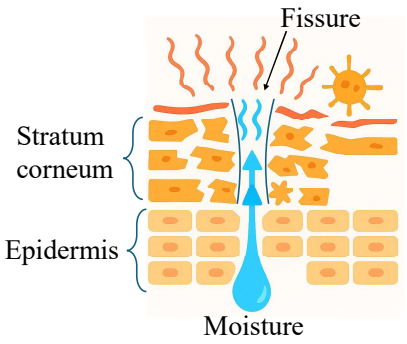

Fig. 1. Sketch of the skin cross-section affected by AD. Fissures and cracks are present in the *stratum corneum*, changing the electric properties of the human slab. The figure is not in scale.

Doi: 10.1109/RFID-TA63091.2025.11265920

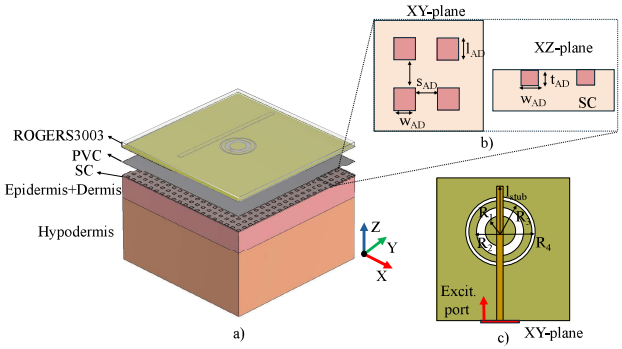

Fig. 2. 3D-view of the loaded AD sensor (a), schematic representation of the AD fissures on the SC layer (b), bottom-view of the proposed AD sensor, with the open-stub feeding line on the upper layer (c). AD-fissures dimension are described by t_{AD}, w_{AD} and l_{AD}, representing the thickness, width and length of fissures, respectively.

TABLE I
CSRR-BASED SENSOR GEOMETRICAL DIMENSIONS

R_1	R_2	R_3	R_4	l_{stub}
0.5	0.8	1	1.1	3

All dimensions are in mm.

This paper presents a resonator-based sensor for AD detection, employing a low-cost CSRR operating in the Ku-band. The high operating frequency enables improved spatial resolution and confines the penetration of the E-field to the upper skin layers (SC and EP), where AD biomarkers are localized. Moreover, a complete description of the human slab, loading the proposed system, is included to obtain an accurate EM-simulation of the problem.

II. MICROSTRIP COUPLED CSRR-BASED DERMATITIS SENSOR

The proposed solution for detecting different AD conditions is based on a near-field resonant structure operating in the Ku-band. As anticipated, AD only affects the outermost layer of the skin, the *stratum corneum*. Due to the vascularization of the dermis and hypodermis, sensing beyond the non-vascularized *stratum corneum* can introduce noise and lead to erroneous detection. Consequently, dermatitis sensors should be designed to specifically target the SC. The sensor adopts a CSRR-structure, excited by an open-end microstrip. The operating principle is based on the interaction of the resonator's near-field fringing field with the SC, which is altered by AD-induced fissures. The proposed multi-layer resonator structure is schematically depicted in Fig. 2, together with the 3D-view of the skin slab adopted in EM simulations, representing the resonator load. The CSRR is patterned on the bottom layer of the sensor and positioned to interact with the upper skin layer, where fissures of varying t_{AD} and w_{AD} (see Fig. 2(b)) appear depending on AD severity. To enable a contact-less structure, a thin layer (10 µm) of Polyvinyl chloride (PVC) is inserted between the skin slab and the resonator. To avoid direct electrical contact with the skin, the

TABLE II
GEOMETRIC AND ELECTRIC PROPERTIES OF THE SKIN SLAB AT 16 GHZ

Skin layer	Thickness (mm)	ϵ'	σ (S/m)
SC	0.015	3.9	0.65
Epidermis	0.05	23.4	15.19
Dermis	1.4	23.4	15.19
Hypodermis	4.3	6.51	4.4

CSRR is excited via an open-ended microstrip line on the top layer, while the resonator is placed on the bottom. A 16 GHz operating frequency is chosen as a trade-off between high spatial resolution for AD detection and fabrication feasibility in a miniaturized design. To set the sensor operating frequency, both the open-stub length (l_{stub}) and the CSRR parameters are optimized. The resulting sensor geometrical parameters are detailed in Table I. Electrical and geometrical properties of the multilayer skin slab are taken from the literature [10], [11], and derived for the adopted operating frequency using the Djordjevic-Sarkar dispersion model, as reported in Table II. A representative healthy skin model (without AD) is initially adopted as the load of the sensor to be designed. Full-wave simulations of the loaded sensor, carried out in the CST Studio environment, predict both the reflection coefficient at the excitation port shown in Fig. 2 and the E-field penetration of the loaded resonator. For the healthy SC case, EM-simulations predict a -36 dB reflection coefficient magnitude at 16 GHz. To verify that the interaction between the E-field, excited by the CSRR, and the skin slab is only superficial, the mean value of the discrete samples of the E-field norm, taken over an XY area approximately corresponding to the square circumscribed around the CSRR, is monitored for a set of penetration levels z_k along the Z-direction. These values are normalized to the corresponding maximum and calculated as follows:

$$\langle \|\mathbf{E}(z_k)\| \rangle = \frac{1}{N_x N_y} \sum_{i=1}^{N_x} \sum_{j=1}^{N_y} \left(\frac{\|\mathbf{E}(x_i, y_j, z_k)\|}{\max_k \|\mathbf{E}(z_k)\|} \right) \quad (1)$$

where N_x and N_y are the number of cells along X-and Y-directions, respectively, while z_k identifies the longitudinal position of the k-th XY-plane. The predicted results are shown in Fig. 3: as anticipated, AD affects only the SC layer; therefore, the E-field intensity in deeper layers does not influence the sensor read-out, avoiding misleading readings. From Fig. 3, it can be evinced that the E-field intensity is maximum at the interface between the resonator and the PVC layer, while at the interface with the SC a 20% decrease is observed; a 50% reduction is observed inside the SC layer, while after 30 µm the mean value of the E-field norm is only 10% of the maximum value.

III. EM-SIMULATION OF THE ATOPIC DERMATITIS SENSOR: DETECTION MECHANISM AND SENSITIVITY ANALYSIS

The previously designed CSRR-based system is subsequently loaded with a multi-layer skin model, in

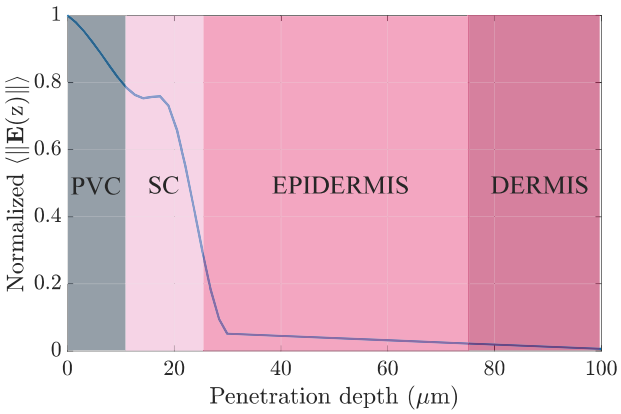

Fig. 3. EM-simulated mean value of the normalized E-field norm, along the penetration direction, for the AD-free-skin case (t_{AD} = w_{AD} = 0). The graph is truncated at z_k= 100 µm since the E-field is negligible at deeper penetration depths.

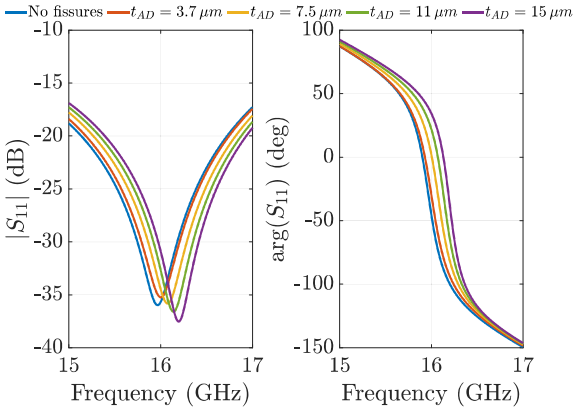

Fig. 4. Simulated reflection coefficient (in magnitude and phase) of the loaded CSRR-resonator, for varying SC fissure thicknesses. Distinct trends can be observed in both components. The healthy-skin case is also reported for a clearer comparison.

which the *stratum corneum* is suitably defected, to emulate various AD-induced fissure conditions. Specifically, different fissure thicknesses, referred to as the parameter t_{AD}, and different fissure widths, indicated as w_{AD}, are introduced, and a systematic procedure is established to analyze the corresponding electromagnetic simulation results. By examining both the variations in the S_{11} parameter and the E-field distribution within the multilayer structure, the system effectively distinguishes between different levels of AD severity. For the proposed AD detection system, the planar sensor is designed to be in full contact with the skin, without any air gap. However, due to the rapid decay of the electric field within the skin slab, the presence of air between the *stratum corneum* and the resonator could affect the sensor read-out. Therefore, firm adhesion between the device and the skin is critical for accurate detection. In both of the following sections AD affected SC-regions are modeled as small air cavities.

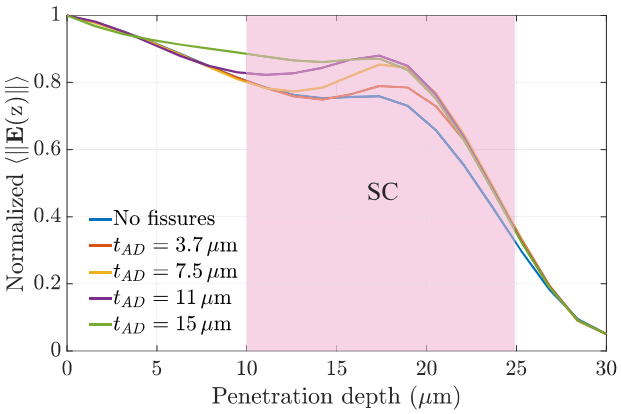

Fig. 5. EM-simulated normalized E-field norm along the first 30 µm, for varying fissures thickness: t_{AD}= 0 µm corresponds to the healthy skin case, while t_{AD} = 15 µm to a fully damaged SC, with w_{AD} = l_{AD} = 200 µm.

A. Detection of Variable AD Fissure Thickness

Firstly, EM-simulations are performed to evaluate the behavior of both S_{11} and $\langle\|\mathbf{E}(z)\|\rangle$ with respect to varying fissures thickness, t_{AD} (see Fig. 2). In the proposed analysis, t_{AD} is swept from 0 to 15 µm, corresponding to healthy skin and fully damaged skin conditions, respectively. In the proposed scenario, the fissure width, w_{AD}, and length, l_{AD}, are set to 200 µm. Fig. 4 shows distinguishable trends in both the magnitude and phase of the sensor S_{11}, demonstrating high sensitivity to AD severity changes: a monotonic frequency shift is observed as the fissures become deeper: the negative peak of the S_{11} is at 15.97 GHz for the healthy skin, and 16.2 GHz for fully damaged SC, showing a 230-MHz frequency shift between the two cases. These results are corroborated by the trend of $\langle\|\mathbf{E}(z)\|\rangle$ with respect to t_{AD} variations, as shown in Fig. 5. Notably, $\langle\|\mathbf{E}(z)\|\rangle$ vanishes beyond the SC layer even in AD-affected skin, indicating negligible influence from deeper layers and distinct penetration behaviors for different t_{AD}. Higher t_{AD} values, associated with deeper fissures, reduce the SC effective conductivity and thus increase EM-field penetration depth.

B. Detection of Variable AD Fissure Width

A similar analysis is conducted for varying widths of the SC fissures, while l_{AD} and t_{AD} are fixed at 200 µm and 11 µm, respectively. As in the case of varying t_{AD}, both S_{11} and the $\langle\|\mathbf{E}(z)\|\rangle$ are monitored. Fig. 6 shows the magnitude and phase of the reflection coefficient for w_{AD} ranging from 0.1 to 0.3 mm, demonstrating the capabilities of the sensor to detect fractures caused by AD also over the XY-plane. In particular, an up-frequency shift is observed with increasing fissure width: for w_{AD} = 0.1 mm, the resonance remains at the nominal operating frequency of 16 GHz, while for w_{AD} = 0.3 mm a 150-MHz frequency shift is predicted. As for the varying t_{AD} cases, similar considerations regarding the E-field penetration depth can be derived for the w_{AD} scenario. As shown in Fig. 7, the larger the fissure width, the deeper

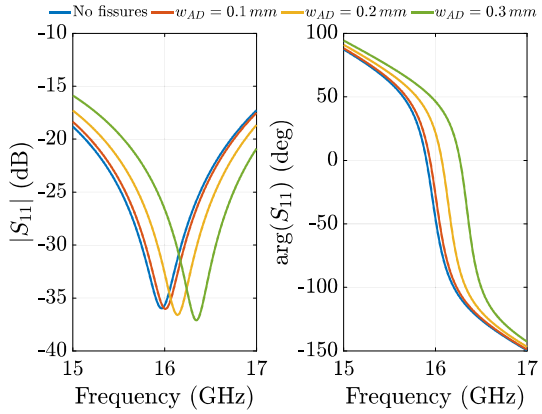

Fig. 6. Simulated reflection coefficient (in magnitude and phase) of the loaded CSRR-resonator, for varying SC fissure widths in the 0.1 to 0.3 µm range.

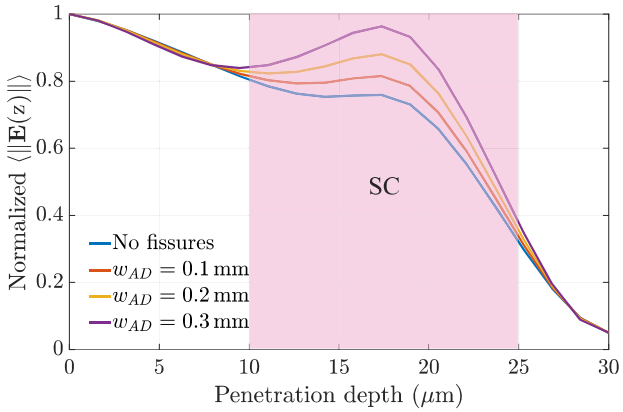

Fig. 7. EM-simulated normalized E-field norm in the first 50 µm for varying fissure thickness. 0 µm corresponds to the healthy skin case, while 15 µm to a fully damaged SC, with t_{AD} = 11 µm.

the electric field penetrates the skin slab, due to the resonator interaction with a larger volume of air.

This selective dependence of the electromagnetic field on the thickness and width of the fissures can be used as a fundamental result in the development of an ad-hoc machine learning algorithm for real-time skin health condition detection, given the large amount of data that can be provided as input for model training [12].

C. Sensor Sensitivity to Variations in AD Severity

The sensor sensitivity for a generic variation in the geometrical parameter d (in this case, thickness and width) can be evaluated as:

$$S_{\mathrm{d}} = \frac{\Delta f_{\mathrm{res}}}{\Delta d} = \frac{f_{\mathrm{res},i+1} - f_{\mathrm{res},i}}{d_{i+1} - d_i} \quad \left(\frac{\mathrm{MHz}}{\mu\mathrm{m}}\right) \tag{2}$$

where $f_{\mathrm{res},i+1}$ and $f_{\mathrm{res},i}$ are the sensor resonant frequencies corresponding to two adjacent values d_{i+1} and d_i of $d \in \{t_{\mathrm{AD}}, w_{\mathrm{AD}}\}$. In the proposed analysis, a representative step-size of 1 µm is used for the t_{AD} variations, and 10 µm for the w_{AD} ones. EM-simulations are carried out to evaluate the worst-case sensitivity for the two fissures geometrical variations, reporting $S_{t_{AD}}$=15 $\frac{\mathrm{MHz}}{\mu\mathrm{m}}$ and $S_{w_{AD}}$=1 $\frac{\mathrm{MHz}}{\mu\mathrm{m}}$, respectively. These values confirm the high responsiveness of the proposed sensor to small structural variations in the SC region.

IV. Conclusion

A miniaturized CSRR, operating in the Ku-band, is designed for AD detection. The high operating frequency confines the sensor fringing E-field to the SC only, where AD biomarkers are located. The sensor concept is evaluated by means of full-wave EM-simulations, where fissures of the SC caused by AD are analyzed by varying their geometry. The skin is modeled as a multilayer structure (SC, EP, DR), with each layer assigned specific geometric and dielectric properties, to ensure an accurate and realistic representation. Furthermore, the selected high operating frequency has the twofold goal of providing an enhanced spatial resolution and of excluding the deeper skin layers, allowing the sensor to present sensitivities of 15 $\frac{\mathrm{MHz}}{\mu\mathrm{m}}$, and 1 $\frac{\mathrm{MHz}}{\mu\mathrm{m}}$ for the thickness and width variations, respectively. The proposed system is compact, lightweight, and miniaturized and can be adapted for the detection of other skin pathologies affecting the *stratum corneum*.

References

[1] Elias PM. The skin barrier as an innate immune element. Semin Immunopathol. 2007 Apr;29(1):3-14.

[2] A. Rizwan et al., "Non-Invasive Hydration Level Estimation in Human Body Using Galvanic Skin Response," in IEEE Sensors Journal, vol. 20, no. 9, pp. 4891-4900, 1 May1, 2020.

[3] J. Kilpijärvi, J. Tolvanen, J. Juuti, N. Halonen and J. Hannu, "A Non-Invasive Method for Hydration Status Measurement With a Microwave Sensor Using Skin Phantoms," in IEEE Sensors Journal, vol. 20, no. 2, pp. 1095-1104, 15 Jan.15, 2020.

[4] M. Baghelani, Z. Abbasi, M. Daneshmand and P. E. Light, "Noninvasive Microwave Sensor for Real-Time Continuous Dehydration Monitoring," in IEEE Sensors Journal, vol. 24, no. 7, pp. 9959-9969, 1 April1, 2024.

[5] A. I. Sunny et al., "Feasibility Experiments to Detect Skin Hydration Using a Bio-Impedance Sensor," 2019 41st Annual International Conference of the IEEE Engineering in Medicine and Biology Society (EMBC), Berlin, Germany, 2019, pp. 6032-6035.

[6] A. Cataldo et al., "Portable Microwave Reflectometry System for Skin Sensing," in IEEE Transactions on Instrumentation and Measurement, vol. 71, pp. 1-8, 2022, Art no. 4003308.

[7] S. Bing, K. Chawang and J. . -C. Chiao, "A Flexible Tuned Radio-Frequency Planar Resonant Loop for Noninvasive Hydration Sensing," in IEEE Journal of Microwaves, vol. 3, no. 1, pp. 181-192, Jan. 2023.

[8] Huang X, Cheng H, Chen K, Zhang Y, Zhang Y, Liu Y, Zhu C, Ouyang SC, Kong GW, Yu C, Huang Y, Rogers JA. Epidermal impedance sensing sheets for precision hydration assessment and spatial mapping. IEEE Trans Biomed Eng. 2013 Oct;60(10):2848-57.

[9] A. R. Todorov et al., "Design of a Flexible, Wearable Interdigitated Capacitive Sensor for Monitoring Biomarkers of Atopic Dermatitis," in IEEE Sensors Journal, vol. 24, no. 5, pp. 6856-6866, 1 March1, 2024.

[10] Sacco, G., Pisa, S. & Zhadobov, M. Age-dependence of electromagnetic power and heat deposition in near-surface tissues in emerging 5G bands. Sci Rep 11, 3983 (2021).

[11] Ziskin, M. C., Alekseev, S. I., Foster, K. R., & Balzano, Q. (2018). Tissue models for RF exposure evaluation at frequencies above 6 GHz. Bioelectromagnetics, 39(3), 173-189.

[12] S. Trovarello, O. Afif, A. Di Florio Di Renzo, D. Masotti, M. Tartagni and A. Costanzo, "A Non-Invasive, Machine Learning Assisted Skin-Hydration Microwave Sensor," 2024 54th European Microwave Conference (EuMC), Paris, France, 2024, pp. 932-935.